Bull. Mater. Sci., Vol. 37, No. 5, August 2014, pp. 983–989. © Indian Academy of Sciences.

Influence of annealing temperature on ZnO thin films grown by dual ion beam sputtering

SUSHIL KUMAR PANDEY[1], SAURABH KUMAR PANDEY[1], VISHNU AWASTHI[1], ASHISH KUMAR[1], UDAY P DESHPANDE[2], MUKUL GUPTA[2] and SHAIBAL MUKHERJEE[1,*]

[1]Discipline of Electrical Engineering, Hybrid Nanodevice Research Group, Indian Institute of Technology, Indore 453 441, India

[2]Department of Atomic Energy (UGC DAE), Consortium for Scientific Research, University Grants Commission, Indore 452 001, India

MS received 4 June 2013; revised 2 July 2013

Abstract. We have investigated the influence of *in situ* annealing on the optical, electrical, structural and morphological properties of ZnO thin films prepared on *p*-type Si(100) substrates by dual ion beam sputtering deposition (DIBSD) system. X-ray diffraction (XRD) measurements showed that all ZnO films have (002) preferred orientation. Full-width at half-maximum (FWHM) of XRD from the (002) crystal plane was observed to reach to a minimum value of 0·139° from ZnO film, annealed at 600 °C. Photoluminescence (PL) measurements demonstrated sharp near-band-edge emission (NBE) at ~ 380 nm along with broad deep level emissions (DLEs) at room temperature. Moreover, when the annealing temperature was increased from 400 to 600 °C, the ratio of NBE peak intensity to DLE peak intensity initially increased, however, it reduced at further increase in annealing temperature. In electrical characterization as well, when annealing temperature was increased from 400 to 600 °C, room temperature electron mobility enhanced from 6·534 to 13·326 cm^2/V s, and then reduced with subsequent increase in temperature. Therefore, 600 °C annealing temperature produced good-quality ZnO film, suitable for optoelectronic devices fabrication. X-ray photoelectron spectroscopy (XPS) study revealed the presence of oxygen interstitials and vacancies point defects in ZnO film annealed at 400 °C.

Keywords. DIBSD; *in situ* annealing; PL; XRD; XPS; ZnO.

1. Introduction

ZnO is extremely popular, primarily because of its wide direct energy bandgap of 3·37 eV (Look 2001). Moreover, as compared to other contemporary wide bandgap semiconductor materials, ZnO offers several fundamental advantages such as (1) high breakdown strength, (2) large excitonic binding energy, (3) availability of native substrate, (4) possibility of performing wet chemical processing, (5) comparatively more resistant to radiation damage and (6) transparency in the visible region (Reynolds *et al* 1996; Look 2001; Look *et al* 2004; Makino *et al* 2005; Pearton *et al* 2005). All these advantages make ZnO thin films and nanostructures suitable for various opto-electronic, photovoltaic device applications (Pearton *et al* 2003). Undoped ZnO thin films shows *n*-type conductivity (Look *et al* 1998; Van de Walle 2000; Pearton *et al* 2003) mainly due to the presence of zinc interstitials (Zn_i) and oxygen vacancies (O_v). Presence of these native defects modifies crystalline properties, which, in turn, primarily affect optical and electrical behaviours of ZnO. Origin of these native defects is strongly dependent not only on ZnO growth conditions, but also on various post-growth treatments such as annealing (Puchert *et al* 1996; Aghamalyan *et al* 2003; Kang *et al* 2004). Therefore, a clear understanding of the effect of native point defects on optical and electrical properties of ZnO is essential for its applications in high-quality electronic and optoelectronic devices. Due to large lattice mismatch between Si(100) and ZnO, obtaining high-quality ZnO films on Si substrate is challenging. But growth of ZnO films on Si substrates is critically important in terms of realizing cost-effective and large-scale fabrication of optoelectronic and photovoltaic devices.

There are a number of deposition techniques such as pulsed laser deposition, sputtering and chemical vapour deposition to grow ZnO thin films (Zhao *et al* 2005; Yu *et al* 2009). Among these, dual ion beam sputtering deposition (DIBSD) system is noteworthy to produce high-quality thin films with comparatively superior compositional stoichiometry, uniformity and adhesion to the substrate even for films grown at room temperature. Besides these, other salient features of the DIBSD system

*Author for correspondence (shaibal@iiti.ac.in)

are high-quality growth with reduced surface roughness on a larger substrate area; *in situ* substrate pre-cleaning before carrying out the growth process. Therefore, a clear understanding of the influence of *in situ* annealing treatment on ZnO properties is extremely important. To the best of our knowledge, there has not been any report on *in situ* ultra-high vacuum annealing study of ZnO thin films grown by dual ion beam sputtering.

In this paper, an elaborate investigation was carried out to improve electrical, optical, elemental, structural and morphological properties of ZnO thin films grown on Si(100) substrate by performing post-growth *in situ* annealing inside the DIBSD deposition chamber. PL, Hall measurements, XRD, XPS and AFM measurements were carried out to determine optical, electrical, crystalline, elemental and morphological properties of annealed ZnO films, respectively.

2. Experimental

Elettrorava DIBSD system (Pandey *et al* 2013) was deployed to deposit ZnO thin films on *p*-Si(100) substrates. The angle between the sputtering beam and the ZnO sputtering target was fixed at 45° off normal, while the angle between the assist ion beam and the substrate was maintained at 60°. Before inserting into the DIBSD growth chamber, Si(100) substrates were rinsed thoroughly with trichloroethylene, acetone, iso-propanol and de-ionized (DI) water and subsequently purged by 5 N-purity (99·999%) nitrogen gas in order to remove dust particles and various organic contaminants. Prior to actual film deposition, assist source was turned on for 10 min to perform substrate pre-cleaning by Ar ion bombardment. During material growth, assist ion beam, consisting of a plasma of Ar and O_2 ions, helped in the reduction of columnar growth and thereby enhancing growth uniformity and film adhesion to the substrate. The discharge voltage and current of the assist ion source was kept constant at 70 V and 600 mA, respectively, during ZnO thin film deposition, using a 4 N (99·99%) pure 4-in-diameter ZnO target mounted on a water-cooled target holder inside the DIBSD system chamber. The background pressure inside the process chamber was maintained at around 1×10^{-8} mbar, while the working pressure during film growth was kept at $3{\cdot}26 \times 10^{-4}$ mbar.

ZnO materials grown at 400 °C in a gas ambient of $O_2/(O_2 + Ar)$% of 66·67% with radio-frequency (RF) power of 60 W were used to study the effect of *in situ* vacuum ($\sim 1 \times 10^{-8}$ mbar) annealing on the behaviour of ZnO thin films. Annealing temperature was varied from 400 to 800 °C for 30 min with a substrate rotation of 10 rpm. The surface morphology of ZnO films was measured by Veeco Atomic Force Microscope (AFM). Dong-Woo Optron PL set-up, affixed with a 20-mW continuous wave (CW) He–Cd laser (excitation wavelength = 325 nm, TEM_{00} mode), 320 and 150 mm focal length monochromators, chopper, lock-in amplifier and a photomultiplier tube (PMT) detector, was deployed to conduct optical studies of annealed ZnO films. Crystalline nature of the annealed ZnO thin films was investigated using Bruker D8 Advance X-ray diffractometer (CuKα, $\lambda = 0{\cdot}1541$ nm). The stoichiometry of the ZnO film annealed at 400 °C was analysed by X-ray photoelectron spectroscopy (XPS), utilizing a PHOIBOS 100 analyser with AlKα radiation (1486·6 eV) as an excitation source. The sample surface was etched using 1 keV Ar ions beam before measuring to remove the air-contaminated top layer. The chemical species were identified through the binding energies. The binding energies were determined by fitting the XPS spectral line shapes with Lorentzian–Gaussian functions. Room temperature electrical properties were measured using four-probe Hall measurement set-up in Van der Pauw geometry with a magnetic field of 0·50 Tesla.

3. Results and discussion

3.1 *Structural properties*

Figure 1(a) demonstrated the variation of XRD spectra from ZnO films for different annealing temperatures. It should be mentioned at this point that ZnO films, which were considered for *in situ* annealing studies, were grown at 400 °C substrate temperature with $O_2/(O_2 + Ar)$% of 66·67% and RF power 60 W. The crystal structure of ZnO films annealed at various substrate temperatures ranging from 400 to 800 °C was identified to be *c*-axis oriented. The position of (002) peak was observed to decrease consistently from 34·630° for the film annealed at 400 to 34·552 °C for the film annealed at 700 °C and then somewhat increased to 34·554° for the film annealed at 800 °C substrate temperature. It is already well known that the angular peak position of ZnO powder is located at 34·42° (Pandey *et al* 2013). The shift in the corresponding diffraction peak position for different annealing temperatures might have been caused due to stress changing in the film. The angular peak positions of the film grown at 400 °C is higher than that of the ZnO powder peak; indicating that the lattice constant, *c*, of the ZnO film was less as compared to that of the ZnO single crystal, and the unit cells were under tensile stress. It was also observed that with an increase in annealing temperature, the peak position of (002) plane shifted towards the angular value of ZnO powder peak. The peak position became 34·552° at annealing temperature of 700 °C. However, for higher annealing temperature, such as 800 °C, the (002) peak position was again observed to slightly enhance from the angular value of powder peak, indicating increase in stress of ZnO films.

The *c*-axis constant was obtained from Bragg diffraction angle of the (002) peak and was used to evaluate stress on ZnO films (Kumar *et al* 2008).

$$\sigma = -4{\cdot}5 \times 10^{12} \{(c - c_0)/c_0\}. \quad (1)$$

Crystallite size was also calculated from the well-known Scherrer's formula (Cullity 1979):

$$D = 0{\cdot}9\lambda/(A \cos \theta), \quad (2)$$

where λ is X-ray wavelength, A the full-width at half-maximum (FWHM) of the (002) diffraction peak in radians and θ the Bragg diffraction angle of the (002) peak.

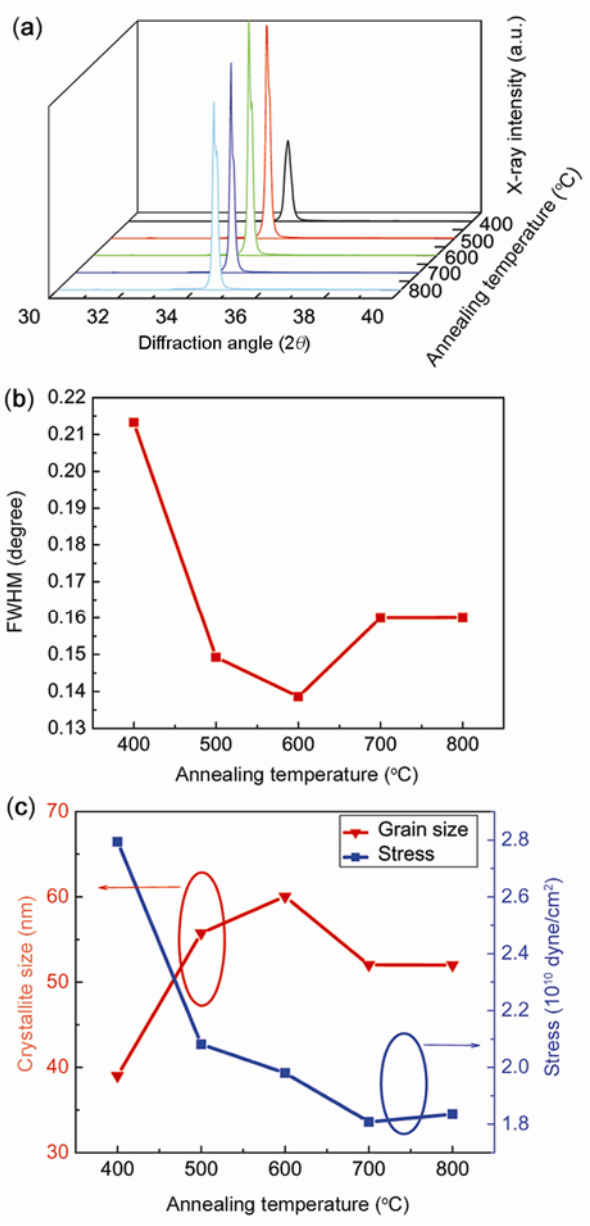

Figure 1. (**a**) XRD patterns of ZnO (002) peaks, (**b**) FWHM of ZnO (002) peaks and (**c**) crystallite size and stress generation on ZnO thin films grown at 400 °C, RF power = 60 W, $O_2/(O_2 + Ar)$% of 66·67% for different annealing temperatures.

Figure 1(b–c) describes FWHM of (002) diffraction peak, crystallite size and stress in ZnO films for different *in situ* post-growth annealing temperatures. Figure 1(b) illustrates FWHM of ZnO (002) diffraction peak. It was found that ZnO film, annealed at 600 °C, had a minimum value of 0·139° for FWHM. Numerical results showed that ZnO crystallite size, as could be illustrated in figure 1(c), was the minimum with a value of ~ 39 nm at 400 °C and maximum with a value of ~ 60 nm at 600 °C. As observed in figure 1(c), stress on films decreased from $2{\cdot}79 \times 10^{10}$ to $1{\cdot}81 \times 10^{10}$ dyne/cm^2 as annealing temperature increased from 400 to 700 °C and then, increased to $1{\cdot}84 \times 10^{10}$ dyne/cm^2 as annealing temperature rose to 800 °C. At low-annealing temperature, surface atoms had less energy and, thus, the surface mobility of atoms was low, resulting in generation of defects in ZnO films. As annealing temperature was increased, those atoms gained sufficient kinetic energy and surface mobility to occupy stable positions inside ZnO crystals. This helped in enhancement of crystalline property of ZnO thin films. Further increase in annealing temperature resulted in breaking of ZnO bonds rather than enabling the atoms to move freely to their corresponding stable sites, producing defects and stress in ZnO film (Kim *et al* 1997).

Figure 2 depicts surface morphology of ZnO films, as characterized by AFM measurements. Root-mean-square (RMS) roughness for 5×5 μm^2 area was observed to decrease from 17·57 Å at 400 °C to 12·64 Å at 500 °C, and, then, increased gradually to 40·92 Å, when annealing temperature was enhanced to 800 °C.

3.2 *Optical properties*

Optical properties of the ZnO films were analysed by PL measurement set-up, affixed with a 20-mW continuous wave (CW) He–Cd laser (excitation wavelength = 325 nm, TEM_{00} mode), monochromators, chopper, lock-in amplifier and a photomultiplier tube (PMT) detector. Figure 3(a–b) described the variation of PL intensity and the ratio of NBE to DLE with spectral wavelength for different annealing temperatures. Excitonic NBE was observed at ~ 380 nm, corresponding to the band gap of ZnO (~ 3·3 eV) at room temperature for all ZnO thin films grown on Si(100). Apart from the excitonic emission in the ultraviolet region of electromagnetic spectrum, a broad PL intensity in the visible region due to DLE was also observed in ZnO samples, as could be observed in figure 3(a). The ratio of NBE emission peak intensity to DLE peak intensity increased with annealing temperatures ranging from 400 to 600 °C and, thereafter, decreased with further increase in annealing temperature. That exactly followed the trend of ZnO (002) XRD peak intensity variation with different annealing temperatures, as

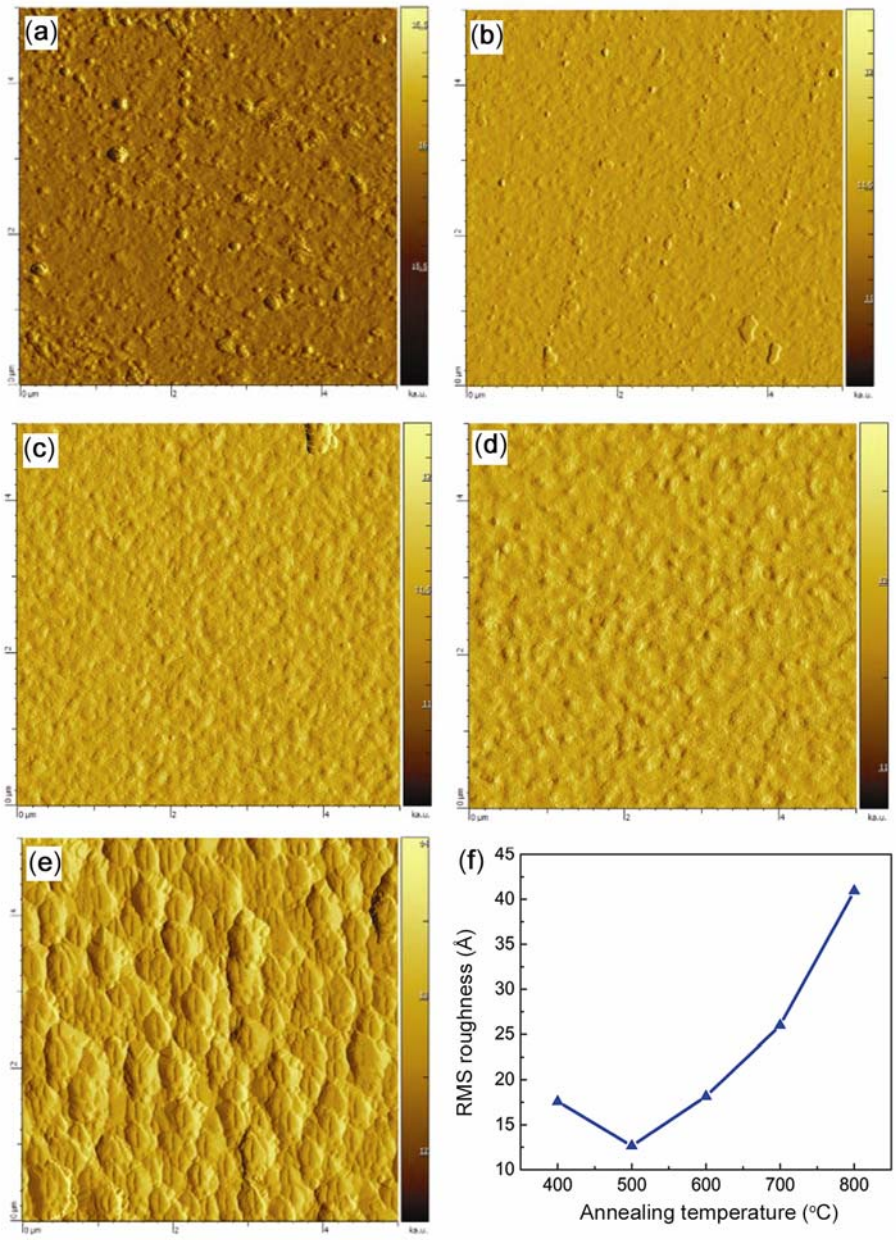

Figure 2. AFM images (5 × 5 μm) of ZnO films annealed at (**a**) 400, (**b**) 500, (**c**) 600, (**d**) 700 and (**e**) 800 °C, (**f**) surface RMS roughness (5 × 5 μm) of ZnO thin films annealed at temperature range of 400–800 °C.

shown in figure 1(a). Moreover, the improved ratio of NBE to DLE actually indicated an improvement of ZnO crystalline quality, as previously confirmed by XRD measurements.

DLE from ZnO film was quite broad and was observed to be centred at ~485 nm (bluish-green) and ~560 nm (yellowish-green). In principle, visible photo-emission from ZnO originates from defects present in the film. The origin of bluish-green emission had mainly been attributed to the presence of oxygen vacancies and zinc interstitials (Kroger and Vink 1954; Vanheusden *et al* 1996; Vanheusden *et al* 1997; Studenikin *et al* 1998; Leiter *et al* 2001; Zhang *et al* 2007) in ZnO crystals. The origin of yellowish-green emission had mainly been attributed to the presence of oxygen interstitials and zinc vacancies in ZnO crystals (Kroger and Vink 1954; Vanheusden *et al* 1996, 1997; Studenikin *et al* 1998; Leiter *et al* 2001; Zhang *et al* 2007). At the beginning, as *in situ* annealing temperature increased from 400 to 600 °C, DLE peaks shifted from 560 to 545 nm and the peak intensity of NBE from ZnO film improved. However, the intensity of DLE emission decreased with increase in annealing temperature from 400 to 600 °C, and this signifies the reduction in defects in ZnO crystal with improved

crystallinity, as predicted by XRD measurements. NBE peak intensity was the maximum at 700 °C annealing temperature, however, DLE peak was also found to be higher as compared to that from ZnO annealed at lower temperatures. This signifies the formation of defects at higher annealing temperatures.

3.3 *Electrical properties*

Four-probe Hall measurements considering van der Pauw geometry were carried out with a magnetic field of 0·50 tesla at room temperature in order to formulate free electron concentration, Hall mobility and electrical resistivity of ZnO films. The variation of electrical properties of ZnO films, annealed at various substrate temperatures, is illustrated in figure 4. It is well known that oxygen vacancies and zinc interstitials act as donor type defects in ZnO crystal (Look *et al* 1998; Pearton *et al* 2003). ZnO film, annealed at 400 °C, was found to have the highest electron concentration of $7{\cdot}247 \times 10^{18}$ cm^{-3} with carrier mobility of 6·534 cm^2/V s at room temperature with resistivity of 0·132 ohm-cm. This high electron concentration was primarily attributed to native donor defects in ZnO film. Free electron concentration was found to have a minimum value of $1{\cdot}426 \times 10^{17}$ cm^{-3} from ZnO annealed at 600 °C. This was justified by PL spectra, as in figure 3, in which DLE peak intensity, originated due to the presence of native crystal defects, was minimum at 600 °C annealing temperature. Electron concentration increased with further enhancement of annealing temperature from 700 to 800 °C, as confirmed by DLE emission in PL measurements.

3.4 *X-ray photoelectron spectroscopy study*

The film stochiometry and defects analysis of the ZnO film was carried out by XPS measurements. Figure 5(a) showed XPS spectra of O 1*s* core level of ZnO thin films annealed at 400 °C substrate temperatures. Individual O1*s* peak had been deconvoluted to generate corresponding

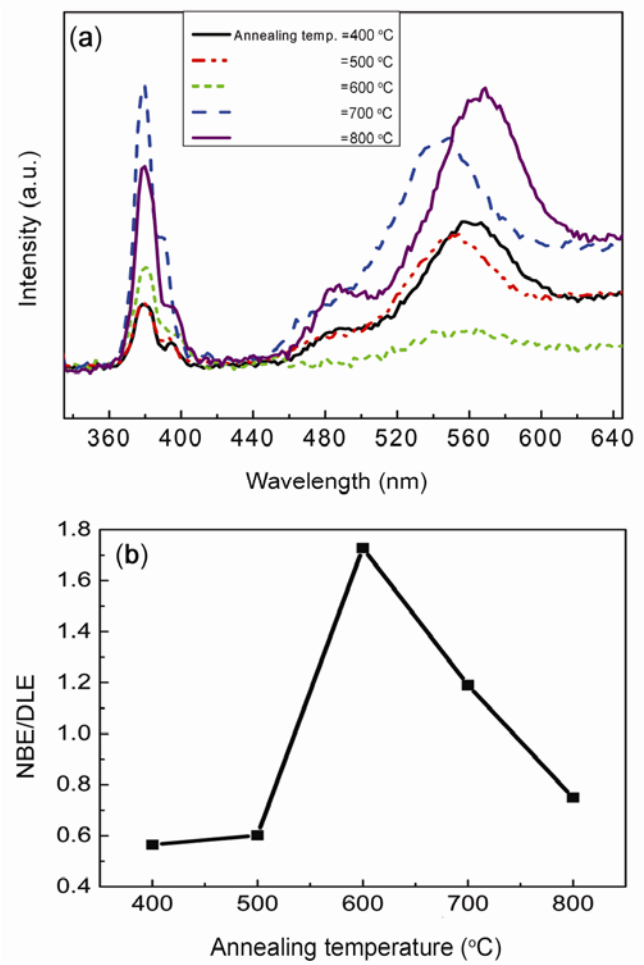

Figure 3. Room-temperature (**a**) PL spectra and (**b**) NBE/DLE for ZnO films annealed at temperature range from 400 to 800 °C.

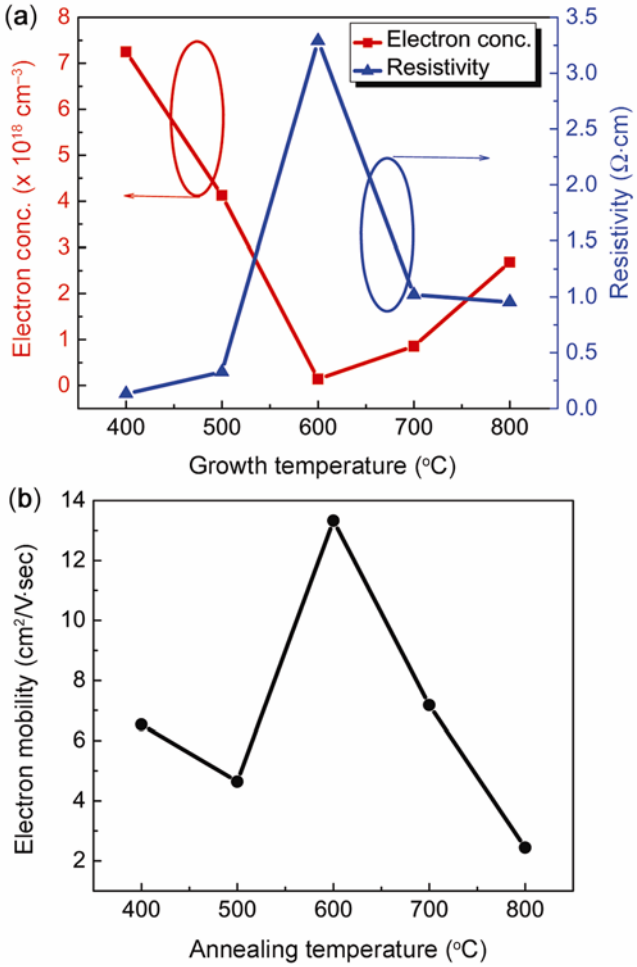

Figure 4. Room temperature (**a**) electron concentration and resistivity and (**b**) mobility of carriers in ZnO thin films annealed at different temperatures.

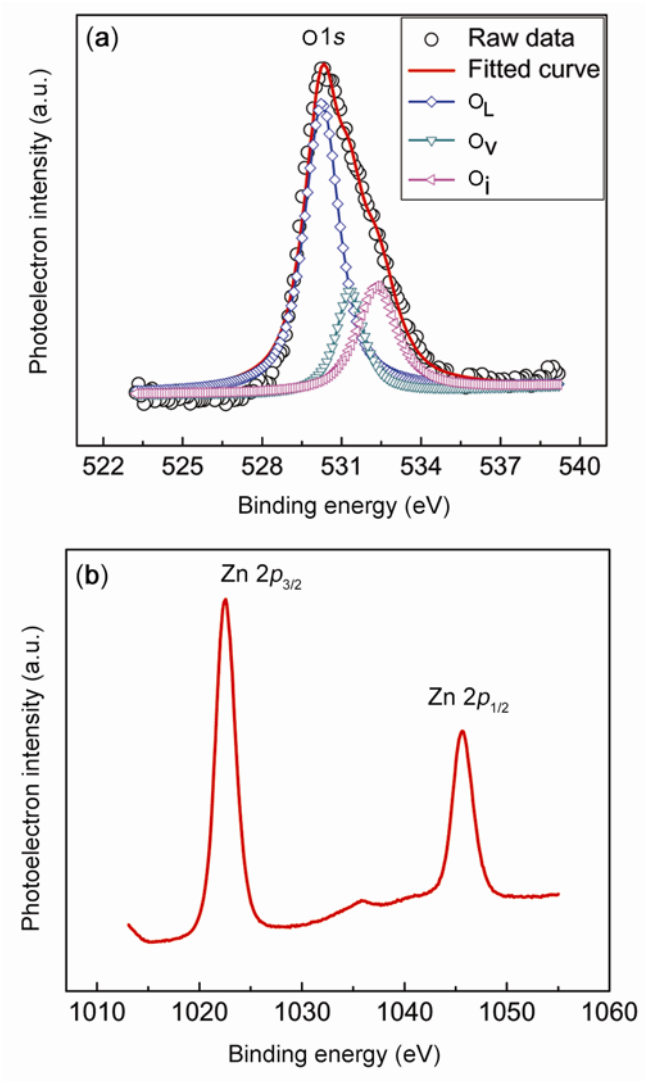

Figure 5. XPS spectra of (**a**) O 1*s* and (**b**) Zn 2*p* for ZnO film annealed at 400 °C.

three distinct, Lorentzian–Gaussian curves centred at binding energies 530·34, 531·28 and 532·41 eV. The low binding energy curve at nearly 530·34 eV is attributed to O atoms at regular lattice site (O_L). The medium binding energy curve at nearly 531·28 eV is associated with O atoms in the oxygen-deficient regions (O_v) within the ZnO matrix. The highest binding energy curve at nearly 532·41 eV corresponds to interstitial O atoms (O_i) or surface oxygen in forms of –OH groups (Islam *et al* 1996; Fan *et al* 2007; Rao *et al* 2010). Figure 5(a) shows that the area of the peak corresponding to O_i is higher than that of the peak corresponding to O_v for the film annealed at 400 °C. This in turn justifies the presence of higher-intensity yellowish-green emission peak (at 560 nm wavelength) as compared to bluish-green emission peak (at 485 nm wavelength) in the PL spectra corresponding to oxygen interstitial (O_i) and oxygen vacancy (O_v) defects, respectively, in the ZnO film. Figure 4(b) demonstrated the XPS spectra of the Zn 2*p* level in ZnO film annealed at 400 °C substrate temperatures. Zn $2p_{3/2}$ and Zn $2p_{1/2}$ peaks were nearly centred at binding energy values of around 1022·41 and around 1045·59 eV, respectively; corresponding to Zn atoms at regular lattice sites in ZnO crystal. The binding energy difference between Zn $2p_{3/2}$ and Zn $2p_{1/2}$ was calculated to be 23·18 eV, which was a characteristic value of ZnO (Islam *et al* 1996; Fan *et al* 2007).

4. Conclusions

In this study, ZnO thin films were grown on *p*-type Si(100) substrates using the DIBSD system. The minimum value of FWHM of XRD from (002) plane was observed to be 0·139° from ZnO film vacuum annealed at 600 °C. It was found that the maximum crystallite size of ZnO thin film, annealed at 600 °C, was ~ 60 nm. AFM analysis showed that the surface roughness of ZnO films gradually reduced to 12·64 Å, on a 5×5 μm scale, as annealing temperature was increased to 500 °C; and then increased with further increase in annealing temperature. The maximum value of electron concentration of $7{\cdot}247 \times 10^{18}$ cm^{-3} with mobility of 6·534 cm^2/V s and resistivity 0·132 ohm-cm were achieved from ZnO film annealed at 400 °C. ZnO film annealed at 600 °C was found to have maximum value of 1·729 for NBE/DLE. XPS analysis confirmed signatures of oxygen interstitials and vacancies defects in the ZnO film annealed at 400 °C. From structural, electrical and optical measurements, it was observed that 600 °C *in situ* annealing temperature was mostly suitable for high-quality ZnO films on Si substrate by DIBSD system for fabrication of optoelectronic devices.

Acknowledgements

This work is partially supported by Department of Science and Technology (DST) Fast Track Scheme for Young Scientist no. SR/FTP/ETA-101/2010. This work is also supported by DST Science and Engineering Research Board (SERB) project number SR/S3/EECE/0142/2011 and Council of Scientific and Industrial Research (CSIR) project number 22(0608)/12/EMR-II. We are also grateful to the atomic force microscopy (AFM) facility equipped at Sophisticated Instrument Centre (SIC), IIT Indore.

References

Aghamalyan N R *et al* 2003 *Semicond. Sci. Technol.* **18** 525

Cullity B D 1979 *Elements of X-ray diffraction* (Reading, MA: Addison-Wesley) 2nd edn

Fan H B, Yang S Y, Zhang P F, Wei H Y, Liu X L, Jiao C M, Zhu Q S, Chen Y H and Wang Z G 2007 *Chin. Phys. Lett.* **24** 2108

Islam M N, Ghosh T B, Chopra K L and Acharya H N 1996 *Thin Solid Films* **280** 20

Kang Hong Seong, Kang Jeong Seok, Kim Jae Won and Lee Sang Yeo 2004 *J. Appl. Phys*. **95** 3

Kim Y J, Kim Y T, Yang H K, Park J C, Han 1 I, Lee Y E and Kim H J 1997 *Vac. Sci. Technol*. **A15** 1103

Kroger F A and Vink H J 1954 *J. Chem. Phys*. **22** 250

Kumar Rajesh, Khare Neeraj, Kumar Vijay and Bhalla G L 2008 *Appl. Surf. Sci.* **254** 6509

Leiter F H, Alves H R, Hofstaetter A, Hofmann D M and Meyer B K 2001 *Phys. Status Solidi* **BR4** 226

Look D C 2001 *Mater. Sci. Eng*. **B80** 383

Look D C, Renlund G M, Burgeber R H and Sizelove J R 2004 *Appl. Phys. Lett*. **85** 5269

Look D C, Reynolds D C, Sizelove J R, Jones R L, Litton C W, Cantwell G and Harsch W C 1998 *Solid State Commun.* **105** 39

Makino T, Segawa Y, Tsukazaki A, Ohtomo A and Kawasaki M 2005 *Appl. Phys. Lett.* **87** 022101

Pandey Sushil Kumar, Pandey Saurabh Kumar, Mukherjee C, Mishra P, Gupta M, Barman S R, D'Souza S W and Mukherjee Shaibal 2013 *J. Mater. Sci.: Mater. Electron.* **24** 2541

Pearton S J, Abernathy C R, Overberg M E, Thaler G T and Norton D P 2003 *J. Appl. Phys.* **93** 1

Pearton S J, Norton D P, Ip K, Heo Y W and Steiner T 2005 *Prog. Mater. Sci.* **50** 293

Puchert M K, Timbrell P Y and Lamb R N 1996 *J. Vac. Sci. Technol*. **A14** 4

Rao T P, Kumar M C S, Safarulla A, Ganesan V, Barman S R and Sanjeeviraja C 2010 *Physica* **B405** 2226

Reynolds D C, Look D C and Jogai B 1996 *Solid State Commun.* **99** 873

Studenikin S A, Golego N and Cocivera M 1998 *J. Appl. Phys*. **84** 2287

Vanheusden K, Seager C H, Warren W L, Trallant D R, Caruso J, Hampden-Smith M J and Kodas T T 1997 *J. Lumin.* **75** 11

Vanheusden K, Warren W L, Seager C H, Trallant D R and Voigt J A 1996 *J. Appl. Phys*. **79** 7983

Van de Walle C G 2000 *Phys. Rev. Lett*. **85** 1012

Yu Chang-Feng, Sung Che-Wei, Chen Sy-Hann and Sun Shih-Jye 2009 *Appl. Surf. Sci.* **256** 792

Zhang J P, Zhang L D, Zhu L Q, Zhang Y, Liu M and Wang X J 2007 *J. Appl. Phys*. **102** 114903

Zhao Jun-Liang, Li Xiao-Min, Bian Ji-Ming, Yu Wei-Dong and Gao Xiang-Dong 2005 *J. Cryst. Growth* **50** 276